Numerical study of the fundamental fiber soliton propagation

H. E. Ibarra-Villalon[a,*], O. Pottiez[b], A. Gómez-Vieyra[a], Y. E. Bracamontes-Rodriguez[b], and J. P. Lauterio-Cruz[c]
[a] *Departamento de Ciencias Básicas. Universidad Autónoma Metropolitana-Unidad Azcapotzalco, Av. San Pablo No. 180. Col. Reynosa Tamaulipas, Azcapotzalco, CDMX. 02200 México.*
[*] *e-mail: uam.hibarra@gmail.com*
[2] *Centro de Investigaciones en Óptica A. C. Lomas del Bosque 115, Col. Lomas del Campestre, León Gto. 37150, México.*
[3] *División de Ciencias e Ingenierías. Universidad de Guanajuato, León Gto. 37150, México.*

Received 1 March 2020; accepted 25 April 2020

This work presents a numerical approach to understand the self-regeneration mechanism of the fundamental soliton propagation driven by the nonlinear Schrödinger equation in the nonlinear fiber formalism. This approach shows that the interplay between dispersion and nonlinearity results in a compensation effect in the phase and the instantaneous frequency representation of the pulse envelope. For a better understanding of this compensation process, 3D mapping propagation graphs are presented.

Keywords: Nonlinear fiber optics; nonlinear Schrödinger equation; optical soliton; chromatic dispersion.

PACS: 42.65.-k; 42.81.Dp; 42.65.Jx

DOI: https://doi.org/10.31349/RevMexFisE.17.191

1. Introduction

Nowadays, soliton-related phenomena are studied in many fields, such as gravitational physics [1], superconductivity theory [2, 3], neurosciences [4], oceanography [5], nonlinear fiber optics [6, 8, 9], among others. The soliton can be viewed as a structure with a self-regeneration mechanism that produces a periodic propagation behavior over a long distance through a specific nonlinear medium. This work is based on the nonlinear fiber optics formalism characterizing the soliton (in a conservative context, known as fundamental soliton) as a light intensity profile (optical pulse) confined in an optical fiber that maintains an invariant envelope over propagation through the interplay of dispersion and nonlinear effects. The latter effects are introduced by the nonlinear response of the optical fiber in the presence of an intense optical field [8–10]. On the other hand, in the same formalism, a soliton can be called dissipative soliton [11] when its intensity profile undergoes over propagation a continuous shaping driven by dissipative processes, in addition to conservative ones; examples of such nonconservative systems are a fiber laser cavity [12] and an optical microresonator [13, 14].

In general, soliton propagation is modeled by a nonlinear partial differential equation, for instance, the complex cubic-quintic Ginzburg-Landau equation (GLE) [9, 11, 12], the nonlinear Korteweg-de Vries equation (KdV) [5, 15, 16], the Gross-Pitaevskii equation (GPE) [17, 18], the sine-Gordon equation [19, 20], the nonlinear Schrödinger equation (NLSE) [6, 8, 9, 18] and others. In this study, we focus on the NLSE that models the optical pulse propagation in an optical fiber. This equation is deduced by a classical Maxwell formalism, considering a quasi-monochromatic electric field with a transversal component (modal distribution in an optical fiber $F(x, y)$) and a longitudinal component (pulse temporal profile $A(z, T) = |A(z, T)| \exp(i\phi(z, T))$), as well as the instantaneous nonlinear response of the optical fiber. This optical medium is viewed as a centrosymmetric material that introduces a third-order susceptibility contribution and third-order nonlinear effects. Adding other considerations taken into account for deducing the NLSE, which are explained in detail in [8, 9], this propagation equation (without losses) writes as

$$\frac{\partial}{\partial z}A(z,T) = -i\frac{\beta_2}{2}\frac{\partial^2}{\partial T^2}A(z,T) + i\gamma|A(z,T)|^2A(z,T) \quad (1)$$

where z is the spatial coordinate, $T = t - z/v_g$ is the temporal coordinate in the frame of reference that moves with the pulse at the group velocity (v_g), β_2 is a parameter that represents the group velocity dispersion and γ is the nonlinear parameter. The first right-hand term is the contribution of chromatic dispersion that introduces a pulse broadening and a delay between the spectral components driven by the dependence of the group velocity of the pulse as a function of the optical frequency [8,9]. The second right-hand term is the nonlinear contribution of the Kerr effect that produces spectral changes and modifies the refractive index as function of the instantaneous intensity ($\propto |A(z, T)|^2$) [8–10, 21]. It is remarkable that the evolution of the temporal profile $A(z, T)$ in Eq. (1) is governed by conservation laws as discussed in [22].

The NLSE in a conservative formalism Eq. (1) can be used to describe multiple dynamics, including modulation instability [23–25], fundamental and high-order solitons [8], dark solitons [8, 26], breathers dynamics [23, 27, 28] and others. In this work, we focus on fundamental solitons whose temporal profiles (hyperbolic secant form) maintain themselves invariant over propagation by a self-regeneration mechanism that relies on the compensation effect taking place in the interplay between dispersion and Kerr effect during the pulse propagation, as discussed in [29]. On the other hand, the fundamental soliton preserves its hyperbolic secant

form when interacts with other pulses of this type, whichin means that if two fundamental solitons collide each other, then this interaction dynamics is driven as an elastic collision process. Thus, it can be argued that the fundamental soliton is robust against perturbations.

In the present work, we analyze the role of the individual contributions of the dispersion and the nonlinearity in the self-regeneration mechanism that explains the invariant temporal profile characterizing the fundamental soliton propagation, as illustrated from an original point of view in Sec. 2. Finally, the conclusions are presented in Sec. 3.

2. Origin of the fundamental fiber soliton propagation

The soliton nature of a pulse propagating in fiber is due to the compensation between the Kerr effect and fiber dispersion in the anomalous regime ($\beta_2 < 0$). To understand this compensation, we follow closely [29] for the study of the NLSE applied to pulse propagation with independent contributions of nonlinear effect and fiber dispersion, for a better understanding of the phenomenology we do not remove the constant phase offsets. In our analysis, we consider a solitary wave solution, describing a first-order soliton ($N = 1$, where N is the soliton order) defined by an initial unchirped hyperbolic secant envelope ($A(z = 0, T) = \sqrt{P_0} sech(T/T_0)$ that is discretized in 2^{10} temporal gridpoints) propagating through a single-mode fiber (SMF-28, $\beta_2 = -21.66$ ps^2/km and $\gamma = 1.5$ /W/km at 1550 nm). A first-order soliton is defined by the principle of the equality between the dispersion length L_D and the nonlinear length L_{NL} ($N^2 = L_D/L_{NL} = 1$; $L_{NL} = 1/(\gamma P0)$; $L_D = T_0^2/|\beta_2| = 1.15$ km, with $T_0 = 5$ ps that it is related with the initial full width at half maximum duration as $T_{FWHM} \approx 1.763T_0$), according to the initial power expressed by $P_0 = 1/(\gamma L_D) = 577.6$ mW.

Firstly, the nonlinear contribution in the NLSE consists of the spatial evolution of the temporal profile in the presence of the Kerr effect that produces changes that depend on the pulse intensity. More precisely, a nonlinear phase proportional to the pulse intensity envelope (self-phase modulation, SPM) affects the pulse temporal profile along z-propagation. This contribution is defined as

$$\frac{\partial}{\partial z} A(z,T) = i\gamma |A(z,T)|^2 A(z,T), \tag{2}$$

Eq. (2) can be solved through the fourth-order Runge-Kutta (RK4) method [30]. The nth step in z-propagation is defined as

$$A(z_n, T_m) = A(z_{n-1}, T_m) + \frac{1}{6} \triangle z(k_1 + 2k_2 + 2k_3 + k_4), \tag{3}$$

where $\triangle\, z = z_n - z_{n-1}$ is the iterative step-size,

$$k_1 = f(A(z_{n-1}, T_m)),$$
$$k_2 = f(A(z_{n-1}, T_m) + 0.5(\triangle z)(k_1)),$$
$$k_3 = f(A(z_{n-1}, T_m) + 0.5(\triangle z)(k_2)),$$
$$k_4 = f(A(z_{n-1}, T_m) + (\triangle z)(k_3)),$$
$$f(A(z,T)) = i\gamma |A(z,T)|^2 A(z,T).$$

We present the temporal profile evolution obtained from the numerical resolution of Eq. (3), as shown in Appendix A, thus the iterative application of the RK4 Eq. (3) models the initial pulse profile ($A(z = 0, T)$) evolution after each $\triangle z$ displacement from the initial position ($z = 0$) to the final propagation distance ($z = 3L_D$). Hence, it is possible to generate a mesh-grid array representation in $(T, z, |A(z,T|^2)$ coordinates that can be depicted as a 3D mapping of the pulse propagation with multicolor scale in the intensity components ($|A(z,T)|^2$). As a result, the 3D mapping of the fundamental soliton propagation shows a sech^2 envelope that remains unchanged over z-propagation, as illustrated in Fig. 1(a). On the other hand, using the fast Fourier transform (FFT) algorithm [30] in Eq. (3), the numerical solution of the pulse propagation can be obtained in the spectral domain, as well as its 3D spectral mapping representation, which shows that the spectral profile presents a broadening, and changes in its shape over $z-$propagation, as illustrated in Fig. 1b). As a basic explanation, it is important to remark that the temporal profile represents a complex quantity ($A(z,T) = |A(z,T)|e^{i\phi(z,T)}$), and the nonlinear contribution in the NLSE provides a nonlinear phase evolution in the temporal domain, which can be calculated as $\phi(z,T) = \phi_{NL}(z,T) = \gamma |A(0,T)|^2 z$ from analytic integration of Eq. (2), as illustrated in Appendix B. The nonlinear phase profile is thus proportional to the pulse intensity profile so that one can say that the pulse profile modulates its phase over propagation, describing the SPM due to the Kerr effect. On the other hand, the Kerr effect alone does not provide any changes in the pulse profile envelope ($|A(z,T)|^2 = A(z,T)A^\dagger(z,T)$), as confirmed by the temporal profile evolution in Fig. 1a), obtained by the numerical resolution of Eq. (3). In contrast, in the spectral domain ($\tilde{A}(z,\omega) = FFT(A(z,T))$), the nonlinear phase contribution introduces changes in the form of a symmetric broadening of the spectral profile, as depicted in Fig. 1b).

Besides, using the four-quadrant inverse tangent ($atan2$) [31] in Eq. (3), the numerical solution of the phase propagation can be calculated in the temporal domain ($\phi(z,T) = atan2(\mathrm{Im}(A(z,T)), \mathrm{Re}\,(A(z,T)))$), as explained in Appendix A. As discussed before, the nonlinear contribution (arising from the Kerr effect) produces the SPM which introduces the nonlinear phase ϕ_{NL}; accordingly, the nonlinear phase evolution obtained numerically shows that a $sech^2$-like profile (proportional to the intensity profile) is reached, with its central value (at $T = 0$ ps) increasing in a linear rate of 1 rad per unit nonlinear length (1 rad$/L_{NL} = 1$ rad$/L_D$), as shown in Fig. 1b). On the other hand, the pulse temporal profile can also be characterized by the instantaneous frequency defined as

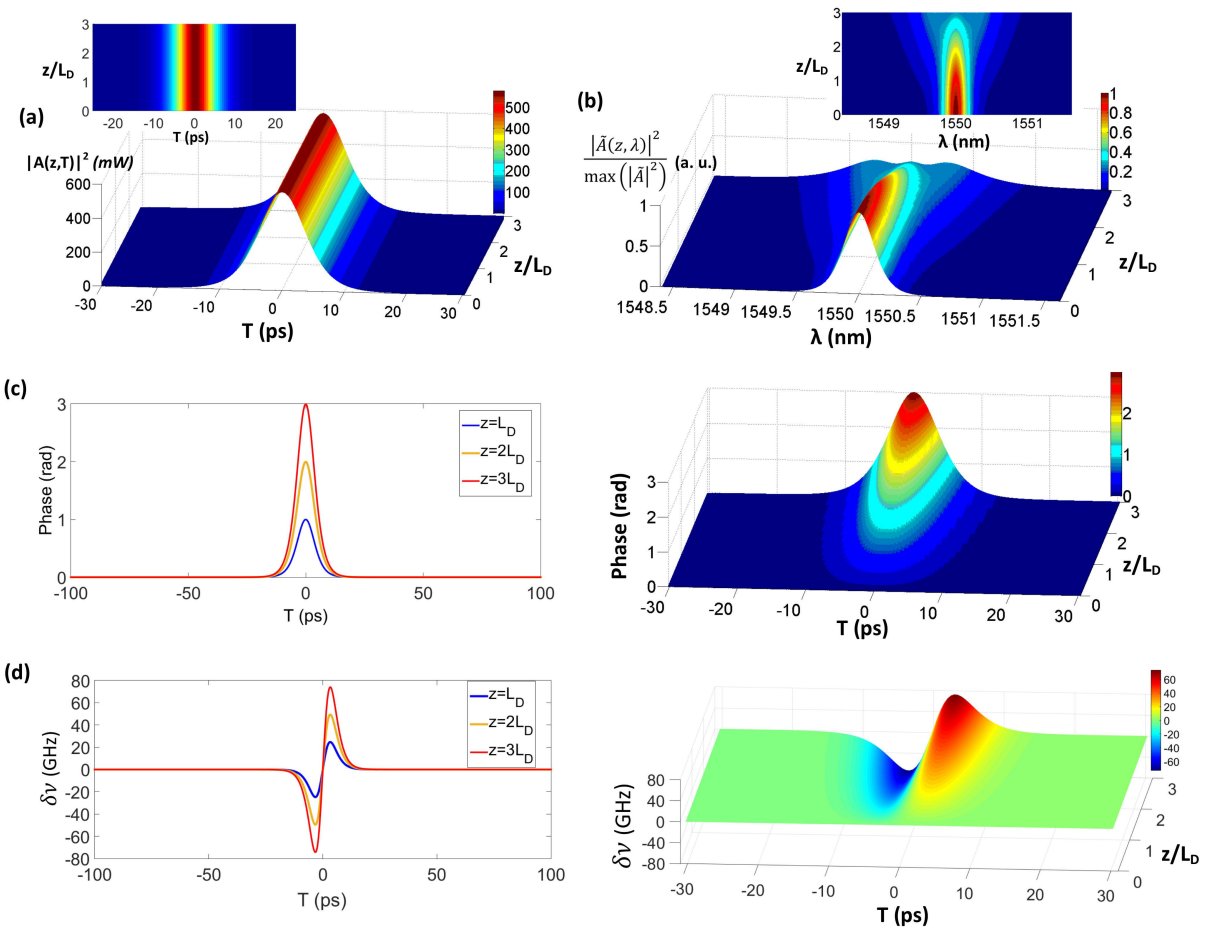

FIGURE 1. Fundamental fiber soliton propagation associated with the nonlinear contribution. a) Temporal profile propagation, b) spectral profile propagation, c) phase evolution and d) instantaneous frequency evolution.

$$\delta\nu = \nu - \nu_0 = -\frac{1}{2\pi}\frac{d}{dT}\phi, \tag{4}$$

where ν_0 ($\lambda_0 = 1550$ nm) is the central frequency of the spectral pulse profile.

As a basic explanation, the instantaneous frequency shows the temporal location of the different spectral components of a signal, that means that the instantaneous frequency can be viewed as a time-frequency mapping; consequently, it is a versatile parameter to understand some physical phenomenologies that involve a signal analysis, as discussed in detail in [32]. In contrast, the pulse propagation problem in optical fiber, as well as in other transparent media, is characterized by a temporal dependence of the instantaneous frequency $\delta\nu = \delta\nu(T)$ that builds up over propagation due to the dispersion contribution and nonlinear effects, this specific dependence $\delta\nu(T)$ is known as "pulse chirp". Hence, the variations in the temporal and spectral pulse profile evolution can be analyzed with the pulse chirp characteristic, which can be used to interpret how the spectral components are distributed along the pulse profile in the temporal domain.

Accordingly, the instantaneous frequency is obtained numerically from Eq. (4), introducing the numerical derivative of the nonlinear phase ($\phi = \phi_{NL}$), as illustrated in Appendix A; for a better accuracy in the numerical derivative, the three points forward difference formula [30] is used. Therefore, the instantaneous frequency representation, as shown in Fig. 1d), describes an S-shaped chirp which defines two regions where the pulse spectral components are localized in the temporal domain. The first region at the leading edge of the temporal profile ($T < 0$) has negative $\delta\nu$ ($\nu < \nu_0$), which means that the red-shifted (longer wavelength) spectral components ($\lambda > \lambda_0$) are localized in this region. The second region at the trailing edge of the temporal profile ($T > 0$) reaches positive values of $\delta\nu$ ($\nu > \nu_0$), meaning that the blue-shifted (shorter-wavelength) spectral components ($\lambda < \lambda_0$) are concentrated in this region. On the other hand, the central region of the instantaneous frequency, which is bounded between the maximum $|\delta\nu|$ values at the leading and trailing edges of the temporal profile, depicts a roughly linear chirp with a positive slope (up chirp). Besides, the validation of the spectral broadening effect induced by the nonlinear contribution is evidenced in the instantaneous frequency representation when the linear chirp evolution increases over propagation. In other words, the generation of new red-shifted and blue-shifted components in the broad-

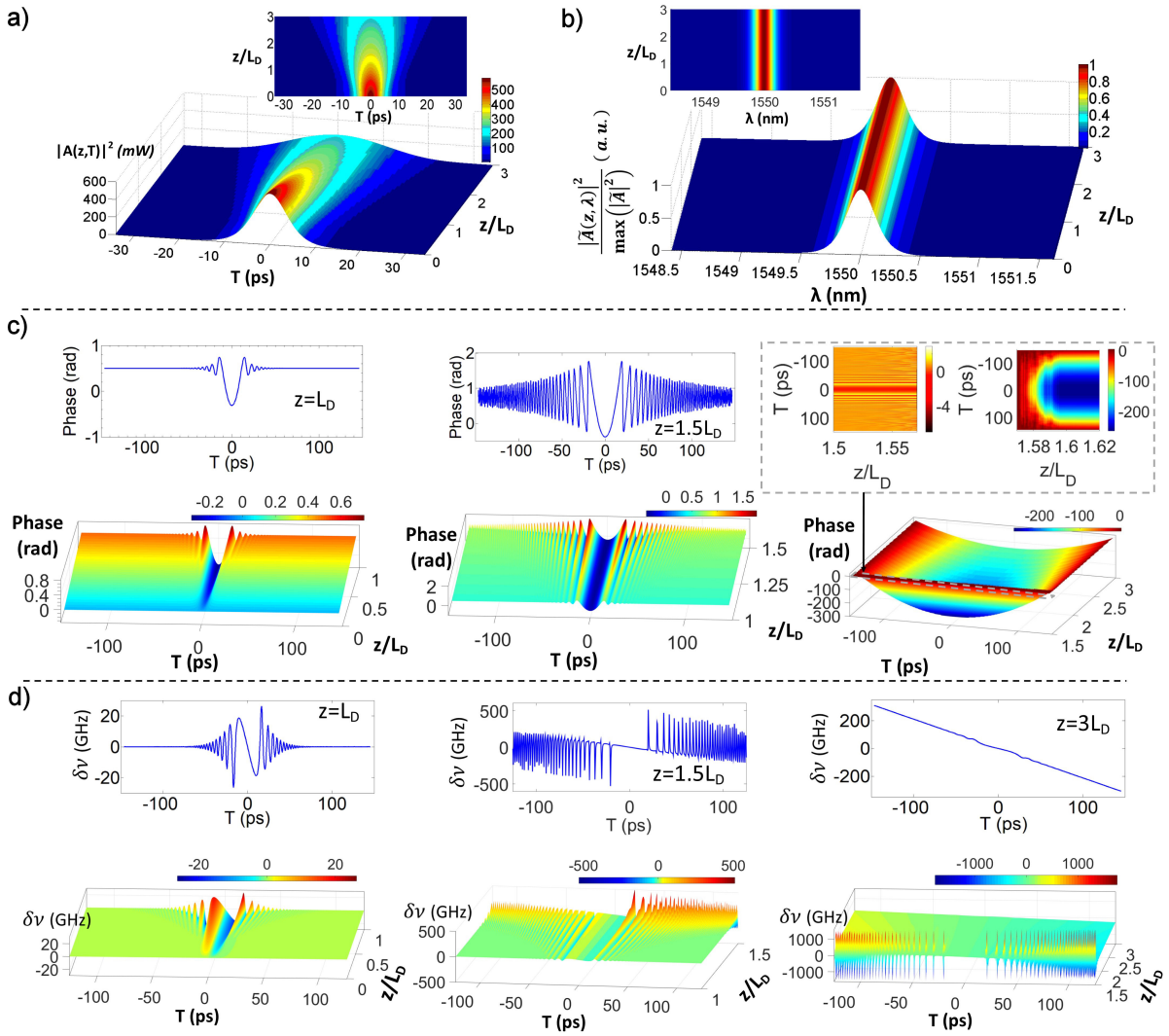

FIGURE 2. Fundamental fiber soliton propagation associated to the dispersion contribution. a) Temporal profile evolution, b) spectral profile evolution, c) phase evolution and d) instantaneous frequency evolution.

ening effect is demonstrated by steepening of the instantaneous frequency and the corresponding increase of the positive linear chirp between the leading and trailing edges of the pulse profile as the maximum $|\delta\nu|$ values increase over propagation; considering that if the maximum $\delta\nu$ value at trailing edge of the temporal profile increases, then new shorter blue-shifted wavelengths are generated; symmetrically, if the minimum $\delta\nu$ value at the leading edge of the temporal profile decreases, then new longer redshifted wavelengths are generated.

On the other hand, the dispersion contribution in a first-order soliton propagation is reproduced by

$$\frac{\partial}{\partial z}A(z,T) = -i\frac{\beta_2}{2}\frac{\partial^2}{\partial T^2}A(z,T), \tag{5}$$

Eq. (5) can be integrated by RK4 in the frequency domain. The nth step over $z-$propagation is defined as:

$$\tilde{A}(z_n,\omega_m) = \tilde{A}(z_{n-1},\omega_m) + \frac{1}{6}\triangle z(d_1+2d_2+2d_3+d_4), \tag{6}$$

where

$$d_1 = g(\tilde{A}(z_{n-1},\omega_m)),$$
$$d_2 = g(\tilde{A}(z_{n-1},\omega_m) + 0.5(\triangle z)(d_1)),$$
$$d_3 = g(\tilde{A}(z_{n-1},\omega_m) + 0.5(\triangle z)(d_2)),$$
$$d_4 = g(\tilde{A}(z_{n-1},\omega_m) + (\triangle z)(d_3)),$$
$$g(\tilde{A}(z,\omega)) = 0.5i\beta_2\omega_m^2\tilde{A}(z,\omega_m).$$

Using the inverse fast Fourier transform ($IFFT$) in Eq. (6), the numerical solution of pulse propagation can be found in the time domain, as discussed in Appendix A; therefore, its 3D mapping evolution (Fig. 2a)) shows that the dispersion contribution alters the pulse temporal profile, broadening it. Besides, the spectral profile is invariant over $z-$propagation (in amplitude), as depicted in Fig. 2b). As a

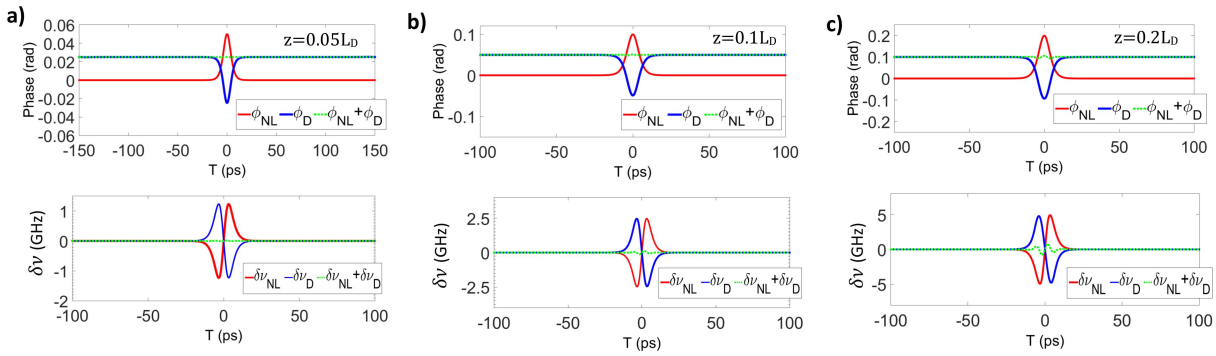

FIGURE 3. Compensation effect between the individual nonlinear and dispersion contributions in the phase and instantaneous frequency after a small propagation distance of: a) $z = 0.05L_D$, b) $z = 0.1L_D$ and c) $z = 0.2L_D$.

basic explanation, the mathematical equation driven by the dispersion contribution Eq. (5) in the spectral domain (replacing $\partial_T \rightarrow -i\omega$) evidences that the dispersion introduces its effect as a spectral phase shift ($\phi_D(z,\lambda)$), as discussed in Appendix B, so the envelope of the spectral profile ($|\tilde{A}(z,\lambda)|^2 = \tilde{A}(z,\lambda)\tilde{A}^{\dagger}(z,\lambda)$, where $\tilde{A}(z,\lambda) = |\tilde{A}(z,\lambda)|e^{i\phi_D(z,\lambda)}$) remains constant over propagation, as validated by the numerical solution in Fig. 2b). In contrast, in the temporal domain ($A(z,T) = IFFT(\tilde{A}(z,\lambda))$), the spectral dispersion phase introduces a symmetric broadening effect in the temporal profile, as confirmed in Fig. 2a).

On the other hand, the tendency of the phase and the instantaneous frequency due to the dispersion contribution are obtained by the same numerical approach as for the case of the nonlinear contribution, as shown in Appendix A; thus, the phase is calculated by the $atan2$ algorithm applied to the temporal profile A(z,T), and the instantaneous frequency by the numerical derivative of the calculated phase, as defined in Eq. (4). Accordingly, the phase evolution shows a profile that modifies its shape and expands over $z-$propagation, as shown in Fig. 2(c); it is notable that for a distance $z < L_D$, the constant phase level at the endpoints of a negative sech^2-like form increases at a linear rate of 0.5 rad$/L_D$; on the other hand, for a distance $z > L_D$ in the constant phase level appears a small ripple that increases over propagation until an induced parabolic phase profile is expanded over all time T range, as depicted in the insets of Fig. 2c).

Also, the instantaneous frequency evolution describes a negative linear slope (chirp < 0) in the central region of the pulse (corresponding to the region of negative sech^2-like form in its phase for $z < L_D$), whose temporal extension is broadening over z-propagation as illustrated in Fig. 2d). A negative chirp is obtained in accordance with the negative value of β_2 (anomalous dispersion regime): indeed, in this regime, the blue-shifted components of the pulse spectrum travel faster than the red-shifted spectral components, so that they separate temporally; as a consequence, the former concentrate in the leading edge of the pulse temporal profile ($T < 0$), and the latter in the trailing edge ($T > 0$), yielding a negative linear chirp. If now β_2 were positive (normal dispersion regime), then the opposite separation would take place, and the chirp would be positive. Thus, it is important to remark that the instantaneous frequency displays an S-shaped form with a negative chirp in the central temporal region of the pulse for $z < L_D$, whereas for $z > L_D$ the instantaneous frequency tends to a negative linear slope with small oscillations that expand over the whole time T range; eventually, these small oscillations disappear over z-propagation until a roughly linear slope is achieved over the whole time range, as depicted Fig. 2d). The negative linear chirp expansion over the whole time range can be understood physically by the distribution of the spectral components over time, according to the linear relationship between arrival time and frequency caused by the anomalous dispersion, this linear relation is defined by the pulse spread function $\delta T = \beta_2 z \delta\nu$, with $\beta_2 < 0$ (anomalous dispersion); thus, the blue-shifted components with positive $\delta\nu$ values shift towards negative times ($\delta T < 0$), whereas the red-shifted components with negative $\delta\nu$ values are delayed towards positive times ($\delta T > 0$).

At a small propagation distance ($z < 0.2L_D$), it is interesting to compare the phase and instantaneous frequency associated with the nonlinear and dispersion effects acting separately, as well the sum of these two contributions, as depicted in Fig. 3. Notably the phase associated with dispersion compensates almost exactly the nonlinear phase; at the same time, the phase introduced by dispersion introduces the constant phase level at the endpoints of the pulse. On the other hand, the negative and positive slopes of the instantaneous frequency in the central region of the pulse (associated with the dispersion and nonlinear contribution, respectively) compensate each other to achieve a nearly constant level. In consequence, if the phase and instantaneous frequency reach a constant and unchirped level in T, then the physical interpretation is that the interplay of the nonlinear effect and dispersion contribution (if the latter is anomalous) allows preserving both temporal and spectral pulse profiles over the propagation. For propagation over longer distances, the compensation is not exact if the two effects are taken separately (see for example the small ripple in the total instantaneous frequency in Fig. 3c)), so it is necessary to analyze the numerical so-

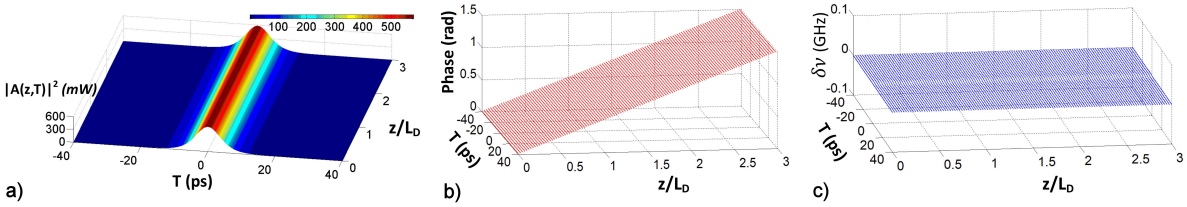

FIGURE 4. Fundamental soliton propagation with both contribution of nonlinear and dispersion part. a) Pulse temporal profile propagation, b) phase evolution, and c) instantaneous frequency evolution over 3 times L_D.

lution with the simultaneous interplay of the nonlinear and dispersion contributions in the NLSE Eq. (1) to get correct results.

In general, when both the nonlinear and dispersion contributions are applied simultaneously in the fundamental soliton propagation, it is possible to compensate for the pulse broadening that occurs in the case of purely anomalous dispersive propagation and to achieve a constant instantaneous frequency over all z-propagation. The latter is explained by the compensation of the positive and negative chirps associated with nonlinear and anomalous dispersion effects, respectively. These characteristics of fundamental soliton propagation are evidenced by the numerical solution of the complete NLSE Eq. (1) solved using a pseudo-spectral method; in particular, we implemented the symmetric split-step Fourier method (S-SSFM) [8]. So, its nth z-step is defined as

$$A(z_n,T) = F^{-1}\left\{ e^{\frac{\Delta z}{2}\tilde{D}} F\left[e^{\Delta z \tilde{N}} F^{-1} \times \left(e^{\frac{\Delta z}{2}\tilde{D}} F(A(z_{n-1},T)) \right) \right] \right\}, \qquad (7)$$

where F and F^{-1} are the fast Fourier transform and its inverse, respectively; $\triangle\, z = z_n - z_{n-1}$ is the spatial step; besides, $\tilde{D} = 0.5i\beta_2\omega^2$ is the linear (dispersion) operator and $\tilde{N} = i\gamma|A(z_{n-1},T)|^2$ is the nonlinear operator.

Firstly, by the numerical solution of the temporal profile of Eq. (7), it can be demonstrated that, in a 3D mapping of the pulse propagation, the sech^2 pulse envelope is preserved over z-propagation, as shown in Fig. 4a). The sech^2 form associated to the nonlinear phase (Fig. 1c)) is compensated by the form associated to the dispersion contribution (Fig. 2c)); therefore, a constant phase (over time) that increases over z at a linear rate of 0.5 rad$/L_D$ is achieved, as depicted in Fig. 4b). As discussed previously, at small propagation distance (Fig. 3), it is clear that the dispersion contribution drives the phase level offsets outside of the central temporal position of the soliton, that increases in a linear rate of 0.5 radian per dispersion length (L_D), whereas the central temporal position of the soliton achieves a constant phase level with the same linear increase rate but the origin is introduced by the simultaneous interplay of the dispersion and the Kerr effect. Finally, if the phase is constant in T, it is clear that the instantaneous frequency (Eq. 4) is zero over the whole temporal profile during $z-$propagation (Fig. 4c)).

3. Conclusions

In general, we have shown that the interplay between the linear and nonlinear parts of the NLSE has an important correlation with each other in order to reproduce a specific phenomenology in the nonlinear fiber optics formalism. In this paper, a complete understanding of the fundamental soliton dynamics modeled by the NLSE that represents a conservative system in the nonlinear fiber optics formalism is studied. It is noticeable that the self-regeneration mechanism of the fundamental soliton is a broadening compensation process between the dispersion contribution and the Kerr effect, which ensures the invariance of the temporal profile over propagation.

Appendix

A. Numerical algorithm to obtain the pulse temporal profile, the phase and instantaneous frequency

To understand the numerical approach used to analyze the fundamental soliton propagation problem, the algorithms to solve the NLSE, as well as to obtain the phase and instantaneous frequency, are presented.

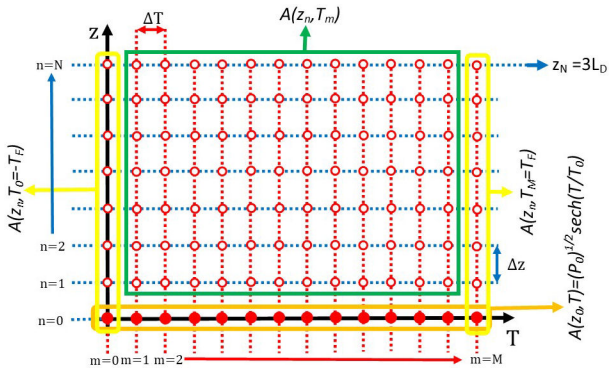

FIGURE A.1. The numerical approach in the fundamental soliton propagation problem. Diagram of the algorithm to solve a) the nonlinear and b) the dispersion contributions of the NLSE. c) Diagram of the split-step Fourier method to solve the NLSE. d) Diagram to obtain numerically the phase and the instantaneous frequency of the pulse temporal profile.

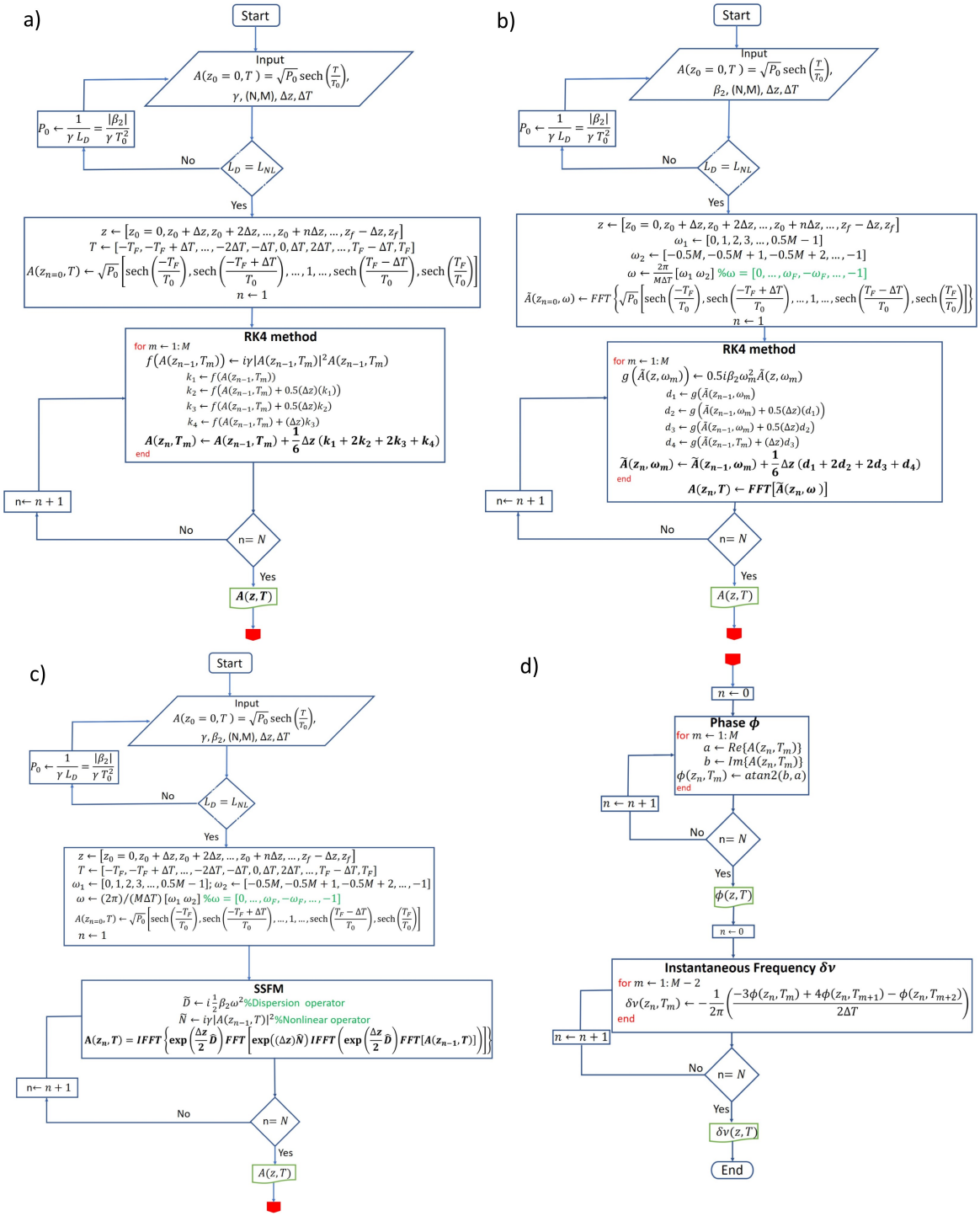

FIGURE A.2. Fundamental fiber soliton propagation associated to the nonlinear contribution. a) Temporal profile propagation, b) spectral profile propagation, c) phase evolution and d) instantaneous frequency evolution.

Firstly, it is important to remark that the numerical solution of the pulse temporal profile is represented by a mesh-grid array in $(z, T, A(z, T))$ coordinates where the z-propagation with $\triangle z$ step is distributed in $N + 1$ levels ($z = [z_0, z_1, ..., z_n, ..., z_{N-1}, z_N]$ where $n \in [0, N]$) and the temporal variable T with $\triangle T$ step is distributed in $M + 1$ elements ($T = [T_0, T_1, ..., T_M, ..., T_{M-1}, T_M]$ where $m \in [0, M]$), as shown in Fig. A.1. To represent the 3D mapping pulse intensity propagation used in this work in Figs. 1a) and 2a), the $A(z, T)$ (complex quantity) coordinate is replaced by $|A(z, T)|^2$ (W). On the other hand, the 3D mapping representation of the pulse intensity profile in the spectral domain (in Figs. 1b) and 2b)) are obtained numerically when the $A(z, T)$

coordinate is replaced by $\tilde{A}(z,\omega) = FFT(A(z,T))$, then $\tilde{A}(z,\omega)$ coordinate is expressed as $|\tilde{A}(z,\lambda)|^2$.

The diagram of the algorithm to solve the nonlinear contribution in the NLSE Eq. (2) is depicted in Fig. A.2a). Firstly, the input parameters are defined, including the initial temporal profile ($A(z_0,T) = \sqrt{P_0}sech(T/T_0)$), the nonlinear parameter (γ), the mesh-grid array size (N,M), the temporal-step size ($\triangle T$) and the z-step size ($\triangle z$). Then, the fundamental soliton condition ($L_D = L_{NL}$) is confirmed; if this condition is not fulfilled, then the initial power is changed to guarantee the fundamental soliton propagation. Additionally, the temporal and spatial distribution are defined ($T \rightarrow [-T_F, ..., 0, ..., T_F]$; $z \rightarrow [0, ..., z_F]$), as well as the initial temporal profile is introduced ($A(0,T) \rightarrow [A(0,-T_F), ..., A(0,0), ..., A(0,T_F)]$). Thus, the RK4 method is applied to integrate Eq. (2) from $z = 0$ to $z = z_F$; ending this iterative process, the pulse temporal profile solution ($A(z,T)$) is reached.

On the other hand, the diagram of the algorithm to solve the dispersion contribution in the NLSE Eq. (5) is shown in Fig. A.2(b). In this case, the diagram follows the same stage description implemented for the nonlinear case, but the NLSE is solved in the spectral domain. Thus it is necessary to introduce the frequency distribution, as well as the initial pulse spectral profile ($\tilde{A}(z_0,\omega) = FFT(A(z_0,T))$); at the same time, the $IFFT$ is used to obtain the pulse profile in the temporal domain.

Besides, the diagram of the algorithm to solve the continuous interplay between the nonlinear and dispersion contribution in the NLSE Eq. (1) is shown in Fig. A.2(c). In this case, the temporal and frequency distributions are introduced to implement the SSFM, which involves integrating the NLSE in the temporal and spectral domain.

Finally, the diagram of the algorithm to obtain numerically the phase and instantaneous frequency is illustrated in Fig. A.2(d). Firstly, implementing the four-quadrant inverse tangent ($atan2$) in the pulse temporal profile solution, the unwrapped phase representation is reached. Then, introducing the numerical derivative of the phase by the three points forwards difference formula, the instantaneous frequency Eq. (4) is gotten.

Note: the presented algorithms can be implemented in multiple computing environments, such as *c, c++, python, GNU OCTAVE*, and others. Also, it is necessary to verify that the discrete representation of the fast Fourier transform (FFT) and its inverse ($IFFT$) are consistent with their continuous representation established in the derivation of the NLSE:

$$\tilde{A}(z,\omega)=FFT(A(z,T)) \leftrightarrow \int_{-\infty}^{\infty} A(z,T)e^{i\omega T}dT \qquad \text{(A.1)}$$

$$A(z,T)=IFFT(\tilde{A}(z,\omega)) \leftrightarrow \int_{-\infty}^{\infty} \tilde{A}(z,\omega)e^{-i\omega T}d\omega. \qquad \text{(A.2)}$$

B. Nonlinear phase and dispersion phase in the pulse propagation problem modeled by the NLSE

To analyze the foundation of the induced phase due to the individual effect of the nonlinear contribution or the dispersion contribution, the next analytic approach is presented.

Firstly, let us introduce a proposed temporal profile expressed as

$$A(z,T) = Ce^{i\phi_{NL}(z,T)}, \qquad \text{(B.1)}$$

where $C = C(T)$ is constant over z-propagation, and ϕ_{NL} is the nonlinear phase.

Then, inserting the proposed temporal profile Eq. (B.1) in the nonlinear contribution of the NLSE Eq. (2), the nonlinear phase is deduced as $\phi_{NL}(z,T) = \gamma|C|^2 z$. Besides, taking into account that the initial temporal profile is known ($A(z=0,T) = C$), thus the nonlinear phase is defined as

$$\phi_{NL}(z,T) = \gamma|A(z=0,T)|^2 z. \qquad \text{(B.2)}$$

In consequence, the nonlinear phase is proportional to the intensity components of the initial temporal profile ($|A(z=0,T)|^2$), the nonlinear parameter ($\gamma = 1.3$ W^{-1} km^{-1} at 1550 nm) and the propagation distance (z). Hence, the nonlinear phase has the same tendency of the initial temporal profile, that means that if a sech^2 initial pulse envelope is considered, then the nonlinear phase depicts a sech^2-like form along the temporal variable T. On the other hand, the nonlinear phase increases over propagation, and it is easy to demonstrated that ϕ_{NL} introduces a linear rate of 1 rad per nonlinear length at the central temporal position of the pulse profile ($T = 0$ ps, where $|A(z=0,T)|^2 = P_0^2$), as demonstrated:

$$\phi_{NL}(z = L_{NL} = L_D, T = 0) = \gamma P_0^2 L_{NL} = 1 \text{ rad}. \qquad \text{(B.3)}$$

On the other hand, the dispersion contribution induced a phase in the spectral domain. Thus, the proposed spectral pulse profile solution is defined as

$$\tilde{A}(z,\omega) = Ge^{i\phi_D(z,\omega)}, \qquad \text{(B.4)}$$

where $G = G(\omega)$ is constant over z-propagation and ϕ_D is the dispersion phase. In the spectral domain, the dispersion contribution is driven by Eq. (5) (replacing $\partial_T \rightarrow -i\omega$) is written as

$$\frac{\partial}{\partial z}\tilde{A}(z,\omega) = i\frac{1}{2}\beta_2\omega^2\tilde{A}(z,\omega). \qquad \text{(B.5)}$$

Thus, inserting the proposed spectral solution Eq. (B.4) in Eq. (B.5), the dispersion phase is expressed mathematically as

$$\phi_D(z,\omega) = \frac{1}{2}\beta_2\omega^2 z. \qquad \text{(B.6)}$$

Accordingly, the dispersion phase is a function of the frequency and z-propagation distance in the spectral domain. In contrast, the dispersion phase in the temporal domain is not easy to define as analytic representation; in consequence, its temporal tendency over propagation is obtained numerically, as analyzed in Sec. 2.

Acknowledgements

This work was funded by CONACyT "Ciencia Básica" project 253925 and H. E. Ibarra Villalón was supported by CONACyT scholar grant (CVU ID: 687612).

1. V. Belinski, E. Verdaguer, *Gravitational Solitons* (Cambridge University Press, Cambridge, 2001), pp. 37-240.
2. A. Bishop, *Solitons and superconductivity, Nat.* **330** (1987) 418, https://doi.org/10.1038/330418a0
3. Y. Tanaka, *Soliton in two-band superconductor, Phys. Rev. Lett.* **88** (2001) 017002, https://doi.org/10.1103/PhysRevLett.88.017002
4. T. Heimburg, A. D. Jackson, *On soliton propagation in biomembranes and nerves, PNAS* **102**(28) (2005) 9790, https://doi.org/10.1073/pnas.0503823102
5. J. R. Apel, *A new analytical model for internal solitons in the ocean, J. Phys. Oceanogr.* **33** (2003) 2247, https://doi.org/10.1175/1520-0485(2003)033⟨2247:ANAMFI⟩2.0.CO;2
6. Y. S. Kivshar, G. Agrawal, *Optical Solitons: From Fibers to Photonic Crystals* (Academic Press, California, USA, 2003), pp. 1-526.
7. N. Akhmediev, A. Ankiewicz, *Dissipative Solitons: From Optics to Biology and Medicine, Lect. Notes Phys. 751* (Springer, Berlin, 2008), pp. 1-474. https://doi.org/10.1007/978-3-540-78217-9
8. G. Agrawal, *Nonlinear Fiber Optics*, 6th ed. (Academic Press, New York, 2019), pp. 1-55.
9. N. Akhmediev, A. Ankiewicz, *Solitons Nonlinear Pulses and Beams* (Chapman and Hall, London, 1997), Chap. 1, 13.
10. R. Paschotta, *Field Guide to Optical Fiber Technology* (SPIE Press, Bellingham, 2010) pp. 33-36.
11. N. Akhmediev, A. Ankiewicz, *Dissipative Solitons, Lect. Notes Phys. 661* (Springer, Berlin Heidelberg, 2005), https://doi.org/10.1007/b11728
12. P. Grelu, N. Akhmediev, *Dissipative solitons for mode-locked lasers, Nat. Photonics* **6**(2) (2012) 84, https://doi.org/10.1038/nphoton.2011.345
13. E. Lucas, M. Karpov, H. Guo, M. L. Gorodetsky, T. J. Kippenberg, *Breathing dissipative solitons in optical microresonators, Nat. Commun.* **8** (2017) 736, https://doi.org/10.1038/s41467-017-00719-w
14. P. Grelu, *Nonlinear Optical Cavity Dynamics: from Microresonators to Fiber Lasers* (Wiley-VCH, Weinheim, 2015), Chap. 6-9.
15. A. Salupere, G. A. Maugin, J. Engelbrecht, J. Kalda, *On the KdV soliton formation and discrete spectral analysis, Wave Motion* **23**(1) (1996) 49, https://doi.org/10.1016/0165-2125(95)00040-2
16. K. W. Chow, R. H. Grimshaw, E. Ding, *Interactions of breathers and solitons in the extended Korteweg-de Vries equation, Wave Motion* **43**(2) (2005) 158, https://doi.org/10.1016/j.wavemoti.2005.09.005
17. R. Atre, P. K. Panigrahi, G. S. Agarwal, *Class of solitary wave solutions of the one-dimensional Gross-Pitaevskii equation, Phys. Rev. E* **73** (2006) 056611, https://doi.org/10.1103/PhysRevE.73.056611
18. X. Antoine, W. Bao, C. Besse, *Computational methods for the dynamics of the nonlinear Schrödinger/Gross-Pitaevskii equations, Comput. Phys. Commun.* **184**(12) (2013) 2621, https://doi.org/10.1016/j.cpc.2013.07.012
19. E. A. Overman II, D. W. McLaughlin, A. R. Bishop, *Coherence and chaos in the driven damped sine-gordon equation: measurement of the soliton spectrum, Physica D* **19**(1) (1986) 1, https://doi.org/10.1016/0167-2789(86)90052-7
20. N. K. Vitanov, *Breather and soliton wave families for the sine-Gordon equation, Proceedings of the Royal Society of London. Series A: Mathematical, Physical and Engineering Sciences* **454** (1998) 2409, https://doi.org/10.1098/rspa.1998.0264
21. P. E. Powers, J. W. Haus, *Fundamentals of Nonlinear Optics*, 2nd ed. (CRC Press, Boca Raton, FL, 2017) pp. 367-369.
22. H. E. Ibarra-Villalon, O. Pottiez, A. Gómez-Vieyra, J. P. Lauterio-Cruz, Y. E. Rodriguez-Bracamontes, *Numerical approaches for solving the nonlinear Schrödinger equation in the nonlinear fiber optics formalism, J. Opt.* **22**(4) (2020) 043501, https://doi.org/10.1088/2040-8986/ab739e
23. S. Boscolo, C. Finot, *Shaping Light in Nonlinear Optical Fiber* (John Wiley & Sons, Chichester, 2017), pp. 1-34.
24. G. P. Agrawal, P. L. Baldeck, R. R. Alfano, *Modulation instability induced by cross-phase modulation in optical fibers, Phys. Rev. A* **39**(7) (1989) 3406, https://doi.org/10.1103/PhysRevA.39.3406
25. J. M. Dudley, G. Genty, F. Dias, B. Kibler, N. Akhmediev, *Modulation instability, Akhmediev Breathers and continuous wave supercontinuum generation, Opt. Express* **17** (2009) 21497, https://doi.org/10.1364/OE.17.021497
26. Y. S. Kivshar, *Dark solitons in nonlinear optics, IEEE J. Quantum Elect.* **29**(1) (1993) 250, https://doi.org/10.1109/3.199266
27. B. Kibler, J. Fatome, C. Finot, G. Millot, F. Dias, G. Genty, N. Akhmediev, J. M. Dudley, *The Peregrine soliton in nonlinear fibre optics, Nat. Phys.* **6**(10) (2010) 790, https://doi.org/10.1038/nphys1740

28. J. M. Dudley, F. Dias, M. Erkintalo, G. Genty, *Instabilities, breathers and rogue waves in optics, Nat. Photonics* **8** (2014) 755. https://doi.org/10.1038/nphoton.2014.220

29. J. M. Dudley, A. C. Peacock, G. Millot, *The cancellation of nonlinear and dispersive phase components on the fundamental optical fiber soliton: a pedagogical note, Opt. Commun.* **193** (2001) 253, https://doi.org/10.1016/S0030-4018(01)01233-0

30. R. S. Esfandiari, *Numerical Methods for Engineers and Scientists using MATLAB®*, 2nd ed. (CRC Press, Boca Raton, Fl, 2017), Chap. 5-7.

31. S. F. Chapman, *Essentials of MATLAB® Programming*, 2nd ed. (Cengage Learning, Boston, 2009) p. 265.

32. B. Boashash, *Estimating and interpreting the instantaneous frequency of a signal- part 1: fundamentals, Proceedings of the IEEE* **80**(4) (1992) 520, https://doi.org/10.1109/5.135376